Icarus 351 (2020) 113943

Contents lists available at ScienceDirect

Icarus

journal homepage: www.elsevier.com/locate/icarus

A possible explanation for the presence of crystalline H_2O-ice on Kuiper Belt objects

Mark J. Loeffler [a,b,*], Patrick D. Tribbett [a], John F. Cooper [c], Steven J. Sturner [d,e]

[a] Department of Astronomy and Planetary Science, Northern Arizona University, Flagstaff, AZ 86011, United States of America
[b] Center for Materials Interfaces in Research and Applications, Northern Arizona University, Flagstaff, AZ 86011, United States of America
[c] Heliospheric Physics Laboratory, NASA Goddard Space Flight Center, Greenbelt, MD 20771, United States of America
[d] Goddard Planetary Heliophysics Institute, University of Maryland, Baltimore County, Baltimore, MD 21228, United States of America
[e] Astroparticle Physics Laboratory, NASA Goddard Space Flight Center, Greenbelt, MD 20771, United States of America

ARTICLE INFO

Keywords:
Astrochemistry
Cosmic rays
Experimental techniques
Ices, IR spectroscopy
Kuiper belt

ABSTRACT

The detection of crystalline H_2O-ice on multiple surfaces of Kuiper Belt Objects (KBOs) seems to contrast with what scientists understand about the surface environment of these objects, as previous estimates suggest that radiolysis should have easily amorphized these objects' surface over their lifetimes. Here, we use a detailed laboratory approach to show that crystalline H_2O-ice can be amorphized by energetic electrons at temperatures as high as 70 K. However, the estimated time needed to completely amorphize the H_2O-ice present on the surface of a KBO to the depth probed by near-infrared spectroscopy is only slightly less than the age of the solar system. Given the uncertainties involved in these types of extrapolations and the possibility of a resurfacing event occurring in these objects lifetime, the detection of crystalline or at least partially crystalline H_2O-ice on KBOs should be expected.

1. Introduction

Crystalline H_2O-ice has been detected on the surface of a variety of objects in our solar system (Pilcher et al., 1972; Fink et al., 1976; Cruikshank, 1980; Grundy et al., 1999; Brown and Calvin, 2000; Jewitt and Luu, 2004; Merlin et al., 2007; Trujillo et al., 2007). The presence of this ordered phase of H_2O-ice has been inferred through the detection of a strong near-infrared absorption feature centered at 1.65 μm (Pilcher et al., 1972; Grundy et al., 1999). Although laboratory studies have shown that this absorption feature is still detectable in amorphous H_2O-ice (Mastrapa and Brown, 2006; Famá et al., 2010), the band is much broader and significantly weaker than its crystalline counterpart, supporting the previous correlation between the strong and sharp 1.65 μm feature and crystalline H_2O-ice.

The persistent detection of crystalline H_2O-ice in the Kuiper Belt (~40 AU) is perplexing (Brown and Calvin, 2000; Jewitt and Luu, 2004; Merlin et al., 2007; Trujillo et al., 2007), given that the surface temperatures of objects in this region are expected to be less than 50 K (Jewitt and Luu, 2004). For instance, laboratory studies have shown that H_2O condensed at these temperatures is amorphous (Sceats and Rice, 1982). While laboratory studies have also shown that amorphous H_2O-ice can crystallize in minutes if it is warmed to higher temperatures found in many extraterrestrial environments (~130 K), extrapolation down to temperatures relevant to Kuiper Belt Objects (KBOs) (<50 K) suggests that expected crystallization times would be longer than the age of the solar system (Jenniskens and Blake, 1996). Nonetheless, even if crystalline H_2O-ice was able to form on these cold objects, it seems likely that energetic particles impacting their surface would tend to amorphize crystalline H_2O-ice.

The assertion that energetic projectiles will amorphize crystalline H_2O-ice originates from numerous studies dating back as much as forty years (e.g., Golecki and Jaccard, 1978; Heide, 1984; Kouchi and Kuroda, 1990; Moore and Hudson, 1992; Strazzulla et al., 1992; Mastrapa and Brown, 2006; Famá et al., 2010). Analytical techniques used with an eye towards astronomical environments have typically focused on either the 1.65 μm absorption band (Leto and Baratta, 2003; Mastrapa and Brown, 2006; Zheng et al., 2009) or the 3.1 μm absorption band (Strazzulla et al., 1992), as both of these absorption bands can be observed via remote sensing. However, another study used the far-infrared absorption band centered at 45 μm (Moore and Hudson, 1992). In addition,

* Corresponding author at: Department of Astronomy and Planetary Science, Northern Arizona University, 527 S. Beaver St, Building 19, Room 209, Flagstaff, AZ 86011, United States of America.
E-mail address: mark.loeffler@nau.edu (M.J. Loeffler).

https://doi.org/10.1016/j.icarus.2020.113943
Received 13 January 2020; Received in revised form 8 June 2020; Accepted 23 June 2020
Available online 30 June 2020

other techniques such as Rutherford backscattering (Golecki and Jaccard, 1978) and electron diffraction (Lepault et al., 1983; Dubochet and Lepault, 1984; Heide, 1984; Kouchi and Kuroda, 1990) have also been used to characterize amorphization of crystalline H_2O-ice. The results from these studies form a mostly self-consistent picture: at the lowest irradiation temperatures crystalline H_2O-ice is completely amorphized, the rate of amorphization decreases rapidly with increasing irradiation temperature and appears to be largely dependent on the total energy absorbed in the sample (Strazzulla et al., 1992; Famá et al., 2010). In addition, there is a critical temperature, where the fraction of crystalline H_2O-ice that can be amorphized begins to decrease. For energetic ions, this temperature appears to vary somewhat between experiments but is likely somewhere around 70–90 K (Moore and Hudson, 1992; Strazzulla et al., 1992; Leto et al., 2005; Famá et al., 2010). For energetic electrons, early studies using electron diffraction showed that 100 keV electrons could amorphize crystalline H_2O-ice up to ~70 K (Lepault et al., 1983; Dubochet and Lepault, 1984; Heide, 1984). However, more recently 5 keV electrons were shown to only partially amorphize crystalline H_2O-ice at 50 K (Zheng et al., 2009), where near-infrared analysis of the 1.65 μm band was used to estimate the crystalline fraction in the sample. Whether the difference observed between these electron irradiation studies is a consequence of the different analytical techniques employed, different electron energies used for irradiation, or another factor is unclear. Nonetheless, the possibility that this critical temperature may be shifted for energetic electrons could potentially explain how crystalline H_2O-ice could survive on the surface of these cold KBOs, where energetic electrons and other particles with low stopping power (dE/dx), are an important component of the radiation flux impinging the surface.

In addition to interest from an astronomical perspective, comparing the limits and efficiencies of amorphization by different particles is also fundamentally interesting. We note that earlier studies aiming to compare effects between energetic ions (hydrogen, helium, and argon) and ultraviolet photons at 16 K have shown that, after scaling to the total energy absorbed in the sample, the rate of amorphization is within a factor of two and the entire sample is amorphized (Leto and Baratta, 2003). The similarity between different projectiles has also been observed when radiation yields have been calculated for new products formed in different astrophysically relevant ice samples (Hudson and Moore, 2001; Baratta et al., 2002; Gerakines et al., 2004; Loeffler et al., 2005). However, as both comparisons described above are typically made at very low temperatures, it is possible that the differences with regards to structural changes become more extreme as the irradiation temperature increases.

The potential difference between energetic electron's and other projectiles' (ions and ultraviolet photons) ability to amorphize crystalline H_2O-ice could have implications for interpretation of the widespread detection of crystalline H_2O-ice on cold KBOs, as well as other cold objects throughout our solar system. Thus, we conducted a set of laboratory studies aimed at characterizing the amorphization of crystalline H_2O-ice induced by energetic electrons. Specifically, we irradiated thin (~55 nm) films of crystalline H_2O-ice with 1–10 keV electrons at 50 K and with 1 keV electrons at temperatures between 10 and 100 K, while monitoring the samples' 3.1 μm absorption band with infrared reflectance spectroscopy. Follow-up irradiation experiments were performed with thicker (~2.17 μm) crystalline H_2O-ice samples, such that the 1.65 μm band could be studied. This combined approach not only allowed us to directly verify that the 1.65 μm band could be effectively used to study amorphization in H_2O-ice but also enabled us to estimate the time needed for amorphization on KBOs, using the sample spectral region probed by remote sensing.

2. Experimental methods

2.1. Experimental setup

All experiments were performed inside a stainless-steel ultra-high vacuum chamber on a radiation-shielded cryostat (Meier and Loeffler, 2020). We have recently modified this system to include infrared spectroscopy (Fig. 1). The base pressure of the chamber was $\sim 3 \times 10^{-9}$ Torr, and inside the radiation shield it is estimated to be 10–100 times lower. Solid H_2O samples were vapor-deposited at near-normal incidence at 150 K with a flux of $\sim 1 \times 10^{15}$ molecules $cm^{-2}\ s^{-1}$ onto an optically flat, gold-mirror electrode of an Inficon IC6 quartz-crystal microbalance (QCM). Depending on the spectral range studied, initial column densities of our irradiated samples were either 1.57×10^{17} molecules cm^{-2} (55 nm) or 6.17×10^{18} molecules cm^{-2} (2.17 μm). Film thicknesses were estimated from our QCM-derived column densities, assuming a density of 0.85 g cm^{-3} for H_2O-ice. We chose this approach, because the number of interference fringes observed during growth of our 55 nm samples (~0.2) prevented us from confidently estimating the film thickness using laser interferometry (Heavens, 1965).

After growth, samples were cooled down to a pre-chosen temperature and irradiated with electrons of a specified energy (1–10 keV) using an EGG-3103C Kimball Physics electron gun aimed at an incident angle of 12.5 degrees. The electron beam was scanned uniformly over an area slightly larger than the crystal to ensure the entire sample was processed. The beam current was measured before and after the irradiation using a Faraday Cup placed in-line with the sample. To prevent loss of secondary electrons from the Faraday Cup, we placed a + 9 V battery in series with the electrometer. During irradiation, the stability of the electron beam was monitored by a thin biased wire collector placed in the electron beam path and biased at −9 V. During the experiments, the beam current typically varied by less than 5%.

The specular reflectance of the H_2O-ice was measured at an incident angle of 37.5°, using a Thermo-Nicolet iS50 Fourier transform infrared spectrometer at 2 cm^{-1} resolution. To obtain a reflectance spectrum of our H_2O-ice sample, we divided the reflectance of the sample (I_{ice}) by the reflectance of the gold mirror substrate taken before film deposition (I_{gold}). The resulting spectrum, $R = I_{ice} / I_{gold}$, was then converted into optical depth, $-\ln R$, before analysis.

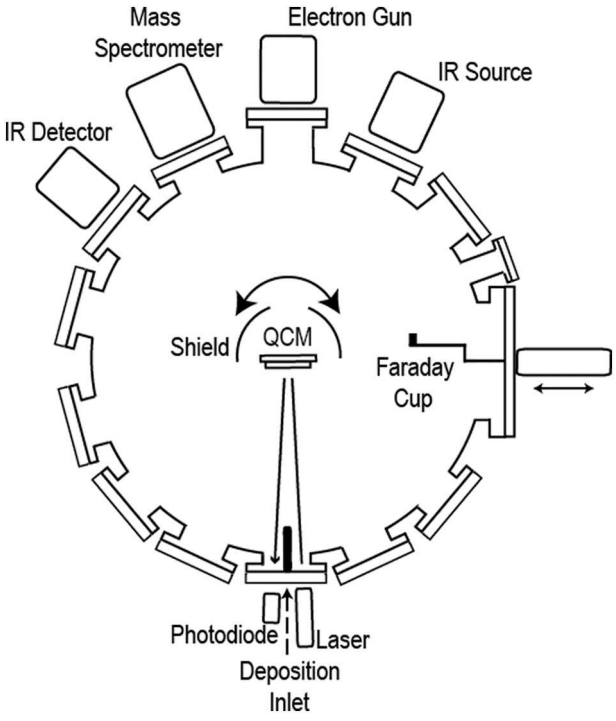

Fig. 1. Experimental setup.

2.2. Reference experiments

A key goal in our experiments is to determine the amorphous fraction of our irradiated crystalline H_2O-ice sample, which relies on comparing its infrared spectrum to the spectrum of amorphous H_2O-ice. Although amorphous H_2O-ice can be produced by vapor depositing H_2O below ~130 K (Sceats and Rice, 1982), the characteristics of the infrared absorption bands of amorphous H_2O-ice can vary slightly with temperature. Thus, we measured reference spectra under conditions as close as possible to that of the irradiated sample, which we discuss below.

For the set of experiments focusing on the 3.1 μm absorption band, we prepared 55 nm films of amorphous H_2O-ice by vapor depositing H_2O at the lowest irradiation temperature (10 K). We subsequently warmed the ice at 1 K / min to the temperature where we performed irradiation. We note that 3.1 μm absorption band warmed from 10 K looked very similar to that of one vapor deposited at the temperature where we performed irradiation (see Fig. 2). This similarity is expected, since the onset of crystallization in amorphous H_2O-ice grown at these low temperatures has been observed to be around ~140–150 K (Pryde and Jones, 1952; Beaumont et al., 1961; Ghormley, 1968; Olander and Rice, 1972; Jenniskens and Blake, 1996), a value that depends strongly on the experimental conditions (see Baragiola (2003) for a review).

For the set of experiments focusing on the 1.65 μm absorption band, we attempted to prepare the 2.17 μm films in the same manner as we did the 55 nm films. However, we found that during warming the near-infrared absorption bands became distorted. Thus, we prepared our reference spectra by depositing at the temperature where irradiation was performed (50 K). The difficulty in growing the thicker reference spectra underscores why there has been some debate regarding the presence of a 1.65 μm absorption in amorphous H_2O-ice (Mastrapa and Brown, 2006; Zheng et al., 2009; Famá et al., 2010). In light of this, we vapor deposited a relatively thin film (1.16×10^{18} H_2O cm^{-2}; 410 nm) at 10 K and warmed it at 1 K / min to 50 K. While this sample thickness may not be ideal for monitoring the amorphous fraction of our sample during irradiation, it was thin enough that the spectral distortion during warming was minimal, allowing us to assess whether the 1.65 μm band was present in amorphous H_2O-ice. These spectra are shown in Fig. 3 and compared with our 2.17 μm samples deposited at 50 K. At 10 K, there is a very weak feature present near the noise level, which, admittedly, by itself may be difficult to identify. However, warming the sample causes this feature to increase slightly, so that it is clearly evident. As in the case of our 55 nm sample, the spectra of the 410 nm sample warmed from 10 K is very similar to the thicker film reference spectra deposited at the higher temperatures.

2.3. Data analysis

Previous studies that have used infrared spectroscopy to quantify the amorphous fraction (φ_a) of crystalline ices during irradiation have typically either fit the spectrum under question with a linear combination of the amorphous and crystalline end members (Moore and Hudson, 1992; Strazzulla et al., 1992; Famá et al., 2010) or evaluated the derivative of the infrared spectrum (Loeffler and Baragiola, 2009; Loeffler et al., 2015), taking advantage of the observation that many features are sharp when the sample is crystalline but broaden as the sample becomes amorphous. We note that a few studies on crystalline H_2O-ice have also attempted to monitor the band area of the 1.65 μm absorption band (Mastrapa and Brown, 2006; Zheng et al., 2009). However, we decided against this approach, because the amorphous sample also contains a broad absorption band in this region, which could lead to an erroneous result (Famá et al., 2010).

Initial analyses of our laboratory data using both the end member and derivative approaches yielded similar results, and thus we opted to use the derivative approach for subsequent analysis of φ_a. Specifically, we quantified the sharpness of the 1.65 μm and 3.1 μm absorption bands by taking the derivative of each spectrum and measuring the peak to peak intensities during irradiation. Fig. 2 (inset) shows an example of the derivative spectrum for the 55 nm H_2O-ice sample irradiated at 50 K, along with the corresponding amorphous spectrum. Using the derivative spectra, we define

$$\varphi_a = 1 - \frac{I_p(F) - I_p(a)}{I_p(0) - I_p(a)} \quad (1)$$

where $I_p(a)$ is the peak to peak intensity of the amorphous spectrum of

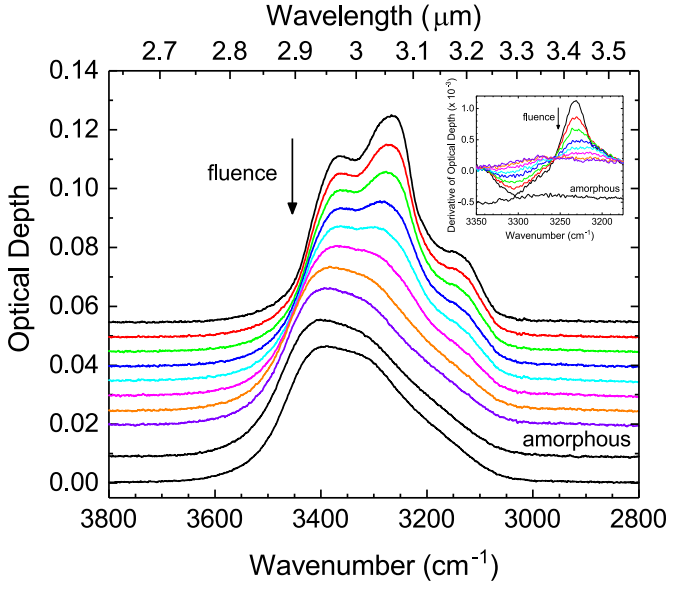

Fig. 2. Infrared spectra of a 1.57×10^{17} H_2O cm^{-2} (55 nm) crystalline sample during irradiation with 1 keV electrons at 50 K compared with that of an amorphous H_2O-ice sample grown at 10 K and warmed to 50 K (2nd from bottom) and deposited at 50 K (bottom). The curves, displaced vertically for clarity, correspond to (from top to bottom) fluences of 0, 1.02, 3.10, 7.22, 12.8, 21.8, 41.0, 323 in units of 10^{14} electrons cm^{-2}. Inset: Corresponding derivative spectra, which were used to quantify the amorphous fraction of the sample.

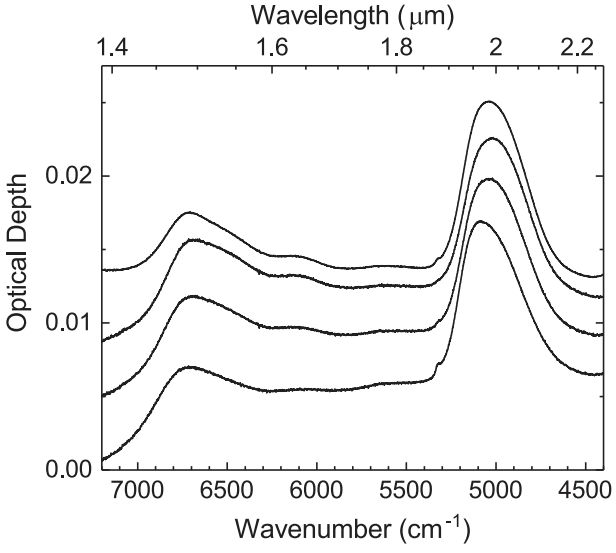

Fig. 3. Near-infrared spectra of amorphous H_2O-ice. The bottom three spectra are a 1.16×10^{18} H_2O cm^{-2} (410 nm) sample deposited at 10 K (bottom) and warmed at 1 K / min to 50 K (2nd from bottom) and 70 K (3rd from bottom). The top spectrum is a 6.18×10^{18} H_2O cm^{-2} (2.17 μm) sample deposited at 50 K. To facilitate better comparison, the top spectrum has been divided by a factor of 3.5.

the sample, which is typically very close to zero, $I_p(0)$ is the peak to peak intensity of the unirradiated sample and $I_p(F)$ is the peak to peak intensity of the sample after a measured electron fluence, F.

2.4. Stopping power and absorbed energy estimates

Since we are interested in comparing the efficiency of amorphization for different electron energies, we need to estimate the total energy absorbed in the sample. We note that over the energy range in our studies (1–10 keV), the energy transferred to our ice sample is overwhelmingly through inelastic collisions within the solid, which is quantified through the inelastic stopping cross section (S_e). To estimate these values, we averaged values of S_e from two publications (Ashley, 1982; Francis et al., 2011) and those calculated from ESTAR (Berger et al., 2005). We note that the values derived from each reference over the energy range used in our study are within ~10% or better of the calculated average.

Another aspect to consider is that the 1–10 keV electrons do not deposit energy uniformly as they pass through our sample, because as they lose energy, S_e increases. Thus, simply multiplying the initial stopping power of the electron (Table 1) by the sample thickness would result in a significant underestimate of the total energy absorbed in the sample. To properly estimate the total energy absorbed in the sample, we wrote an iterative program that integrated the energy transfer to our ice as the electron passes through the sample, assuming a continuously slowing down approximation (CSDA), i.e. that the rate of energy loss along the path is equal to the stopping power (Berger et al., 2005) and internal scattering was negligible. As a test of validity, we used our program to estimate the energy transfer for keV – MeV protons and compared our results to those obtained from SRIM program (Ziegler, 2010), finding excellent agreement between the two. The results for our energetic electrons, along with their initial stopping powers, are given in Table 1.

A final aspect to consider is that in these experiments we are evaluating the phase (amorphous vs. crystalline) of the H_2O-ice sample using infrared spectroscopy, which will probe our entire sample. Thus, we were careful to choose sample thicknesses, where our electrons would pass entirely through the H_2O-ice. An unavoidable consequence of this is that the electrons will interact with our substrate, some being scattered back into the ice and others producing low-energy secondary electrons that can interact with the ice. We estimate that the latter effect will minimally contribute to the total energy absorbed in the sample, as these secondary electrons are, by nature, low energy (~3–5 eV) and that the secondary electron yield from gold at our electron energies is ~1 (Bronshtein and Fraiman, 1969; Walker et al., 2008). On the other hand, over our electron energy range, backscattering of electrons from gold has been measured to be somewhere between 30 and 50% for a sputter-cleaned gold sample (El Gomati et al., 2008). Thus, assuming a worst case scenario (i.e. 50% backscattering), the total energy absorbed value given in Table 1 may be underestimated by as much as 30%.

Table 1
Total energy absorbed.

Energy (keV)	Initial stopping power (eV/nm)[a,b]	Estimated sample thickness[b]	Absorbed energy/ electron (keV)
1	9.6	55 nm	0.644
2	6.1	55 nm	0.362
5	3.2	55 nm	0.179
10	1.9	55 nm	0.103
10	1.9	2.17 μm	5.18

[a] Estimated by taking an average of calculations made by (Ashley, 1982; Berger et al., 2005; Francis et al., 2011).
[b] Assuming density of H_2O-ice is 0.85 g cm^{-3}.

3. Results and discussion

3.1. Amorphization as a function of electron energy

We irradiated crystalline H_2O-ice at 50 K with electrons at energies of 1, 2, 5 and 10 keV, while monitoring the sample with infrared spectroscopy. Fig. 2 shows the evolution of the infrared spectrum for a 1.57 × 10^{17} H_2O cm^{-2} (55 nm) crystalline sample during irradiation with 1 keV electrons. Here, as well as when we irradiated with other energies, irradiation causes the initially sharp features to attenuate until only one broad feature is evident. The resulting spectrum at the end of irradiation closely resembles our reference spectrum of amorphous H_2O (Fig. 2 bottom spectrum), indicating that energetic electrons have amorphized our sample.

Using the approach described in Section 2.3, we determined the amorphous fraction vs. electron fluence at each energy studied (Fig. 4 left). We find that in all cases studied, the sample is amorphized completely, regardless of the electron energy. However, the rate at which our sample is amorphized increases with decreasing energy. For instance, the fluence to amorphize half the sample is ~10 times lower for the 1 keV electrons compared to the 10 keV electrons. This difference is expected, as the 1 keV electrons deposit significantly more energy in the sample (Table 1). Thus, for a better comparison we plot the amorphous fraction of our sample vs. the energy absorbed in our 55 nm film in Fig. 4 (right). After this scaling, the differences between the different irradiation energies are much smaller. For instance, the absorbed energy needed to amorphize the sample is within ~10% for the experiments performed at 1, 2, and 5 keV, while the energy needed in the 10 keV experiment is about 50% higher than the experiments at the lower energies. The similarity observed here is consistent with previous amorphization studies comparing ions and UV photons (Leto and Baratta, 2003), reinforcing earlier suggestions that the main driver of amorphization at low temperatures is the total amount of energy absorbed in the sample.

3.2. Amorphization as a function of temperature

After studying how the amorphization of crystalline H_2O-ice depended on the incident electron energy, we investigated how sensitive amorphization was to the irradiation temperature. In these studies, we irradiated crystalline H_2O-ice with 1 keV electrons at temperatures between 10 and 100 K, while monitoring the sample with infrared spectroscopy. Fig. 5 shows the evolution of the infrared spectrum for a 1.57

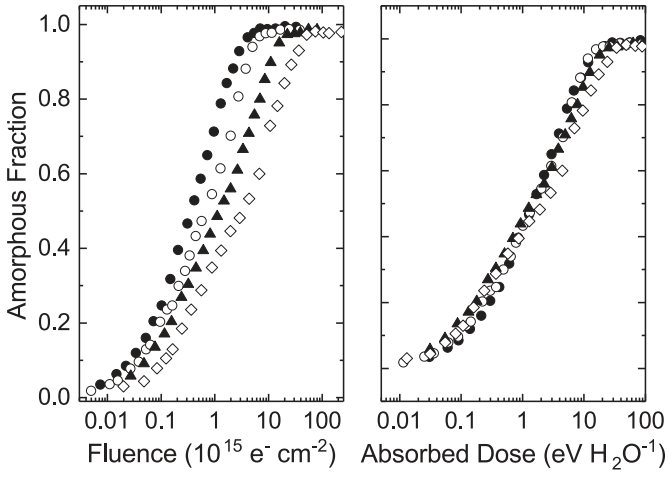

Fig. 4. Fraction of amorphous H_2O vs. electron fluence (left) and absorbed dose (right) during irradiation of a 1.57 × 10^{17} H_2O cm^{-2} (55 nm) crystalline sample at 50 K. Symbols correspond to incident electron energies of 1 (●), 2 (○), 5(▲) and 10 (◊) keV.

$\times 10^{17}$ H_2O cm^{-2} (55 nm) crystalline sample during irradiation at 10 K (top left), 70 K (top right), 80 K (bottom left), and bottom right (100 K). As is the case at 50 K (Fig. 2), the sharper crystalline features of the samples irradiated at 10 and 70 K evolve into one broad feature that closely resembles the reference spectrum of amorphous H_2O sample measured at the irradiation temperature. However, the observed change in the IR spectra at the higher irradiation temperatures (80 and 100 K) is much less significant at the highest fluences studied, as the IR spectrum of the sample irradiated at 80 K still contains sharp absorption features, and the sample irradiated at 100 K closely resembles that of the unirradiated spectrum.

These spectral changes were quantified as in Fig. 4 and are shown in Fig. 6, where we plot the amorphous fraction vs. electron fluence for temperatures between 10 and 100 K. These results indicate that complete amorphization of our sample occurred at temperatures as high as 70 K but the fraction of material that could be amorphized dropped significantly as the temperature was increased above 70 K. For instance, while ~75% of the sample amorphized at 75 K, only ~30% amorphized at 80 K and <10% could be amorphized at 100 K. It is also evident that the rate at which the sample is amorphized is strongly dependent on temperature. For example, the fluence needed to amorphize half the sample is ~60 times lower at 10 K compared with 70 K but only ~3 times lower at 10 K compared with 50 K.

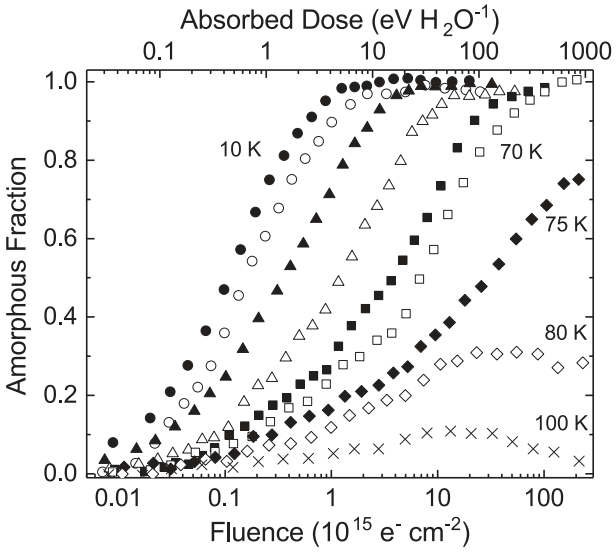

Fig. 6. Fraction of amorphous H_2O vs. electron fluence (bottom) and absorbed dose (top) during irradiation of a 1.57 $\times$ 10^{17} H_2O cm^{-2} (55 nm) crystalline sample with 1 keV electrons at temperatures between 10 and 100 K. Data from left to right at an amorphous fraction of 0.70 correspond to: 10, 30, 50, 60, 65, 70, and 75 K. Experiments at 80 and 100 K are labeled in the figure.

3.3. Amorphization using the 1.65 μm band

Once we established the energy and temperature dependence for

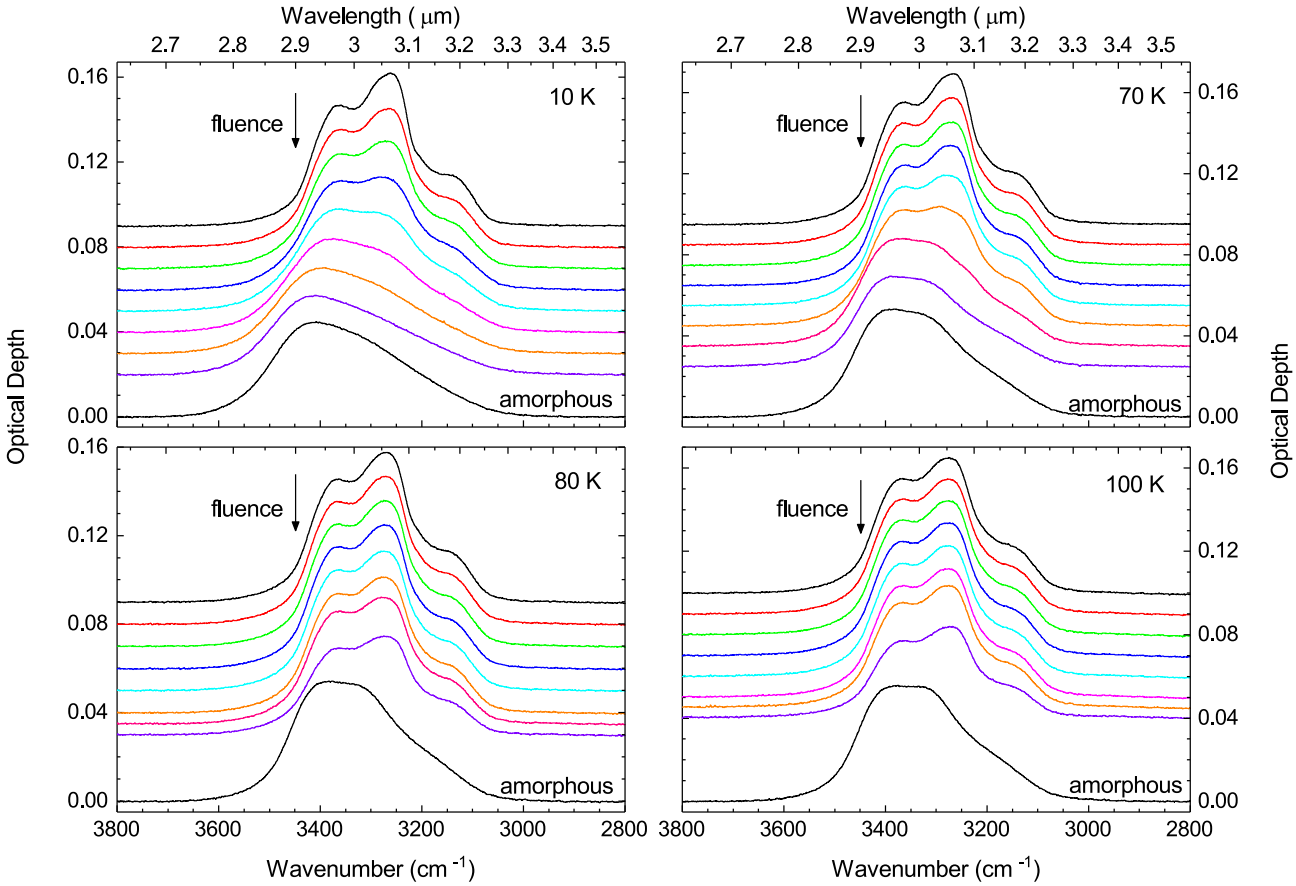

Fig. 5. Infrared spectra of a 1.57 $\times$ 10^{17} H_2O cm^{-2} (55 nm) crystalline sample during irradiation with 1 keV electrons at 10 K (top left), 70 K (top right), 80 K (bottom left), and 100 K (bottom right). All panels show a spectrum of amorphous H_2O-ice sample grown at 10 K and warmed to the respective temperature. The curves, baseline corrected and displaced vertically for clarity, correspond to fluences of (from top to bottom in units of 10^{14} electrons cm^{-2}): top left (10 K): 0, 0.45, 0.98, 1.93, 3.58, 6.52, 12.5, 198; top right (70 K): 0, 1.2, 3.98, 8.96, 50.4, 125, 526, 2030; bottom left (80 K): 0, 1.04, 4.14, 9.95, 49.6, 106, 553, 2320; bottom right (100 K): 0, 1.19, 3.52, 10.4, 49.3, 132, 506, and 2130.

amorphization of the fundamental absorption of H_2O-ice, we turned our attention to the 1.65 μm absorption band, which is often used to characterize the phase of H_2O-ice on objects in the outer solar system. Fig. 7 (top) shows the evolution of the near-infrared spectrum of a 6.17×10^{18} H_2O cm^{-2} (2.17 μm) crystalline sample during irradiation with 10 keV electrons at 50 K. Irradiation causes the sharp feature at 1.65 μm to decrease in intensity and broaden until it closely resembles that of our reference spectrum for an amorphous H_2O-ice sample, consistent with our mid-IR studies as well as previous ones with ion irradiation (Leto et al., 2005; Famá et al., 2010). These spectral changes were quantified as in Figs. 4 and 6; the results for the amorphous fraction vs. electron fluence are shown in Fig. 7 (bottom), where they are overlayed with our mid-IR results at 10 keV. Given that the distribution of deposited energy is different for 55 nm and the 2.17 μm samples, the similarity of the data is quite satisfactory, supporting the assumption that either absorption band can be used quantify the amorphous fraction in H_2O-ice.

3.4. Comparison to previous studies

Besides comparing the amorphization of H_2O-ice using two different spectral regions in our own experimental setup, we can also compare our results with previous studies. Two aspects of interest for comparison are how quickly the sample amorphizes at different temperatures and the approximate temperature when crystalline H_2O-ice can no longer be completely amorphized.

The rate at which the sample amorphizes can be estimated by fitting the experimental data with an exponential function of the form:

$$\varphi_a = \varphi_{a_{max}}\left(1 - e^{-kD}\right) \quad (2)$$

where φ_a is the fraction of amorphized ice, $\varphi_{amax}$is the maximum value of amorphized ice, k is the rate constant in units of molecule eV^{-1} and D is the absorbed dose in units of eV $molecule^{-1}$. We note that although previous studies have typically adopted an equation of the same form as (2), some have used a variable 'K' or 'K^{-1}' to compare amorphization rates (Strazzulla et al., 1992; Famá et al., 2010). To avoid confusion with equilibrium constants, which are typically denoted by 'K', we compare our derived values using 'k' given in (2).

In our experiments, we noticed that the fit shown above got progressively less satisfactory as the irradiation temperature increased. Thus, we also estimated k by determining the dose when 63.2% of the sample had been amorphized (i.e. $kD = 1$). Up to ~60 K, this direct approach yields a k-value within 10% of that derived from the fit but was only within ~30% at temperatures up to 75 K. The derived values from our experiments using the direct extrapolation are shown in Fig. 8 and the error bars indicated the deviation between our direct approach and our fit using (2).

Before we compare our values to those in literature, a few comments are needed. Reports with 100 keV electrons only gave the dose for complete amorphization (Lepault et al., 1983; Dubochet and Lepault, 1984; Heide, 1984). Thus, we adopted the approach used in Famá et al. (2010) to derive k, assuming that $\varphi_a = 0.99$ at the reported fluence and $\varphi_{amax} = 1$. We note that although this approach matches the values given for Heide (1984) in Famá et al. (2010), it is about a factor of eight different for the values given for Dubochet and Lepault (1984). This discrepency is because the values given for Dubochet and Lepault (1984) were taken from an estimate by Strazzulla et al. (1992), assuming that the dose given for amorphization was equivalent to 63.2% of the sample was amorphized ($kD = 1$). The results given in Golecki and Jaccard (1978) were taken by evaluating the dose at which 63.2% of

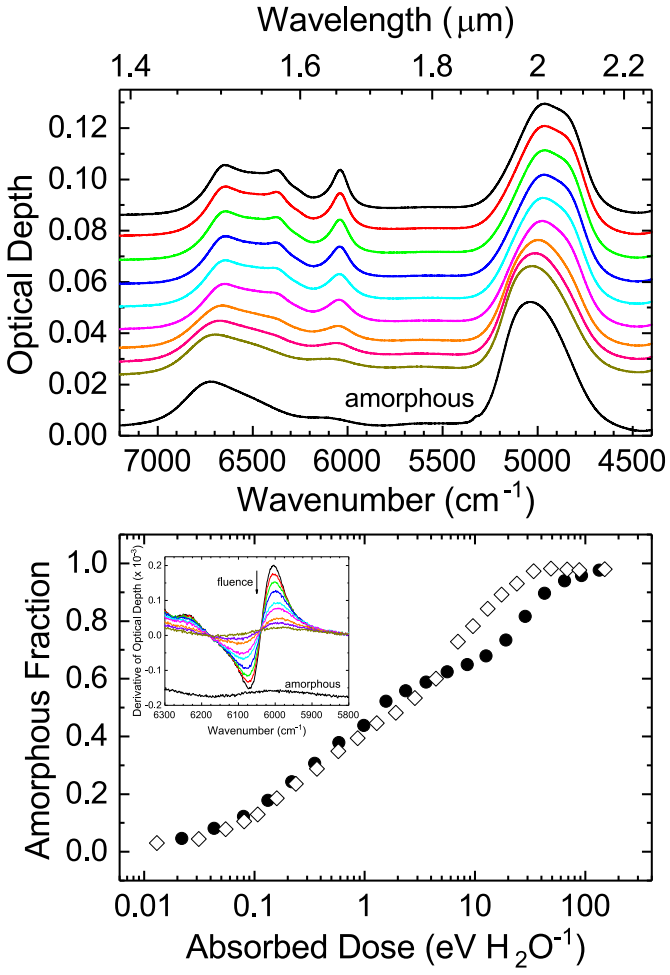

Fig. 7. Top: Near-infrared spectra of a 6.18×10^{18} H_2O cm^{-2} (2.17 μm) crystalline sample during irradiation with 10 keV electrons at 50 K compared with that of an amorphous H_2O-ice sample grown at 50 K. The curves (from top to bottom in units of 10^{14} electrons cm^{-2}), displaced vertically for clarity, correspond to fluences of: 0, 0.95, 2.61, 6.95, 28.0, 101, 341, 510 and 1590. Bottom: fraction of amorphous H_2O vs. absorbed dose during irradiation with 10 keV electrons at 50 K for samples with column densities of 6.18×10^{18} H_2O cm^{-2} (●) and 1.57×10^{17} H_2O cm^{-2} (◇). Inset: corresponding derivative spectra, which were used to quantify the amorphous fraction of the thicker sample (●).

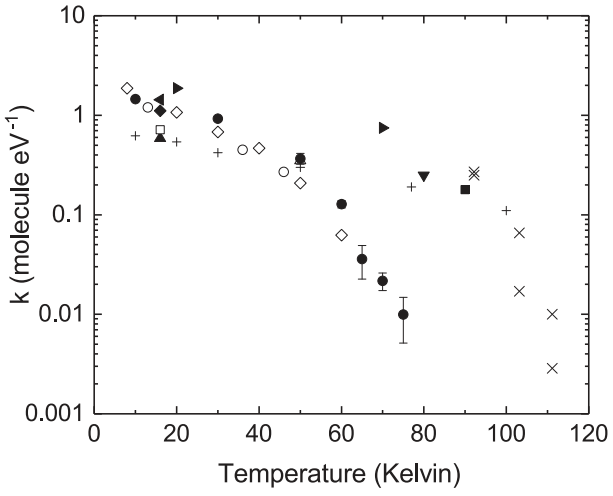

Fig. 8. Comparison of our derived k-value (●) as a function of temperature with previous studies: (×) 100 keV H^+ (Golecki and Jaccard, 1978); (▶)100 keV electrons (Dubochet and Lepault, 1984); (◇) 100 keV electrons (Heide, 1984); (+) 3 keV He^+, (Δ) 1.5 keV H^+ (Strazzulla et al.1992); (○) 700 keV H^+ (Moore et al. 1992); (▲) 30 keV H^+, (□) 30 keV He^+, (◆) 60 keV Ar^{++}, (◂) 10.2 eV photons (Leto and Baratta, 2003); (■) 200 keV H^+ (Leto et al., 2005); (▼) 225 keV H^+ (Famá et al., 2010).

their sample amorphized. Finally, the work by Moore and Hudson (1992) assumed that $\varphi_{amax} = 1$. While this assumption appears to be correct for temperatures ≤46 K, it is unclear whether it holds for higher temperatures, as at the highest doses studied the crystalline fraction is still decreasing. Thus, we only use their values up to 46 K for comparison.

As can be seen in Fig. 8, at low temperatures (< 50 K) k is often similar and no worse than a factor of two to three regardless of projectile, as has been noted previously (Strazzulla et al., 1992; Leto and Baratta, 2003). Our electron irradiation results are consistent with these previous observations. For example, at 50 K our derived k-value varies by about a factor of two between 1 and 10 keV electrons (Table 2) and is no worse than a factor of two compared with estimates for keV He^+ and H^+ ions. The similar k-values for the different projectiles is somewhat surprising given that the density of energy deposition is so different. However, it suggests at these lower temperatures, how quickly the ice structure will reach equilibrium can be reasonably approximated by the total energy absorbed in the sample.

As the irradiation temperature is increased above 50 K, k in our experiments decreases more rapidly, which is consistent with previous studies involving 100 keV electrons (Heide, 1984) and appears to be consistent with the compiled ion irradiation data, although the rapid decrease in k appears to be shifted upwards by ~30 K. However, we note that the rapid decrease at higher temperatures observed for ion irradiation derives from analysis with Rutherford Backscattering Spectrometry (RBS), which was estimated to be sensitive to the top 20–60 nm of the H_2O-ice (Golecki and Jaccard, 1978). As it was shown that amorphization occurred at temperatures as high as ~130 K, we suspect that the damage observed via RBS was not solely structural amorphization but rather a consequence of a compositional change in the irradiated H_2O-ice. Although H_2O-ice is relatively stable under irradiation, the O_2 and H_2 products that form in the sample are largely concentrated near the surface (Teolis et al., 2005; Teolis et al., 2009) and increase with increasing temperature (Boring et al., 1983; Reimann et al., 1984). Thus, these RBS results may be less applicable to amorphization of the entire ice depth as compared to previous studies with infrared spectroscopy, which probed the entire sample depth.

Without the Golecki and Jaccard (1978) data, it appears that the ions show k to decrease steadily with temperature. The cause of differing trend observed between ions and electrons at high temperature is not obvious. However, we speculate that the stopping power (dE/dx) of the projectile becomes an important factor in determining how quickly the sample reaches equilibrium at these higher irradiation temperatures. This may be a consequence of the increase in the sample's specific heat, as described by Famá et al. (2010) in reference to the thermal spike model's explanation of amorphization (Szenes, 1995). Whether the difference in dE/dx for 1 keV electrons (~10 eV / nm) and energetic ions (3 keV He^+, ~200 keV H^+) studied is enough to cause this divergence at higher temperatures is unclear but could be tested in future experiments. In that light, we point out that even though the difference in electronic stopping power is less than a factor of two for 3 keV He^+ studies (~18 eV / nm) and our 1 keV electrons, the nuclear stopping power component for 3 keV He^+ (~16 eV / nm) should drive amorphization, as previous studies have estimated that elastic collisions are ~4 times more efficient than inelastic ones in converting the absorbed energy into heat required for amorphization (Famá et al., 2010).

It is important to point out that k is insightful for comparing how quickly equilibrium in the sample is reached, it gives no information about how much of the sample is amorphized. However, this information can easily be derived by looking at the amorphous fraction of the sample after equilibrium has been reached. Our observation that complete amorphization could only occur ≤70 K is consistent with previous studies using 100 keV electrons (Lepault et al., 1983; Dubochet and Lepault, 1984; Heide, 1984) but is inconsistent with a more recent study using 5 keV electrons that showed only ~40% of the sample could be amorphized at 50 K (Zheng et al., 2009). We suspect that this discrepancy may be partially due to how the crystalline fraction was estimated. In that study, the crystalline fraction was defined as the ratio between the 1.65 μm band area in the irradiated sample and the band area in the unirradiated sample. Yet, as mentioned in Section 2.2, amorphous H_2O-ice has a broad feature in this location at 50 K. Applying this method to our data in Fig. 7, we would have estimated that only ~80% of the sample was amorphized. While this alone cannot explain the apparent discreprency, we note that the 1.65 μm absorption band in crystalline H_2O-ice at 50 K appears to be ~2–3 times stronger in our study than in Zheng et al., 2009. As strength of this absorption band appears to vary among studies (Leto et al., 2005; Mastrapa and Brown, 2006; Famá et al., 2010), it seems reasonable that another method, such as what has been used here or in previous studies (Strazzulla et al., 1992; Famá et al., 2010) would be a more accurate approach to quantify the amorphization of crystalline H_2O-ice.

For energetic ions, a single transition point does not seem to be as well defined as it is with energetic electrons. For instance, although complete amorphization was observed for 3 keV He^+ and 800 keV H^+ at $T < 55$ K, above this temperature the amorphous fraction of the sample was still changing at the end of the experiment (Moore and Hudson, 1992; Strazzulla et al., 1992). However, other experiments using ~200 keV H^+ showed that at the highest temperature studied (80–90 K) complete amorphization of crystalline H_2O-ice was observed (Leto et al., 2005; Famá et al., 2010).

Table 2
Estimated k-value at 50 K.

Energy (keV)	k (H_2O-molecule eV^{-1})[a]
1	0.37
2	0.32
5	0.31
10	0.20 (55 nm ice)
10	0.15 (2.18 μm ice)

[a] Estimated by determining dose, where 63.2% of sample have been amorphized.

4. Astronomical implications

Our results show that crystalline-H_2O ice can be amorphized by irradiation with 1–10 keV electrons at temperatures as high as 70 K, which is consistent with previous studies using 100 keV electron irradiation (Lepault et al., 1983; Dubochet and Lepault, 1984; Heide, 1984), as well as those with keV ion irradiation (Leto et al., 2005; Famá et al., 2010). Thus, we expect that crystalline H_2O-ice present on the surface of an icy body at $T < 70$ K will be amorphized if given a sufficient radiation dose, leaving a weak but broad absorption feature at 1.65 μm. However, as the time needed to accumulate a specific radiation dose can vary significantly, it is not a foregone conclusion that all icy surfaces should be dominated by amorphous H_2O-ice. Below we extrapolate our results, focusing on regions near 40 AU, where icy surfaces are expected to be cold ($T < 50$ K; Jewitt and Luu (2004)) and crystalline H_2O-ice has been detected previously (Brown and Calvin, 2000; Jewitt and Luu, 2004; Merlin et al., 2007; Trujillo et al., 2007).

The estimated radiation flux in this region of the solar system has been estimated previously (Cooper et al., 2003; Strazzulla et al., 2003; Hudson et al., 2008) and is significantly lower than what has been observed on Saturnian and Jovian icy satellites (Cooper et al., 2001; Cooper et al., 2009). In Fig. 9 (left), we provide an updated estimate to the radiation flux for this region of the solar system and also show the derived dosage time vs. depth curve (Fig. 9 right; see Appendix A for details). Clearly, the dosage time vs. depth profile shows a huge variation with depth, sharply decreasing below 0.01 cm and sharply increasing above 100 cm, but nearly constant between these depths. This trend is due to the combination of the flux of heliospheric protons increasing rapidly with decreasing energy below 10 MeV and the

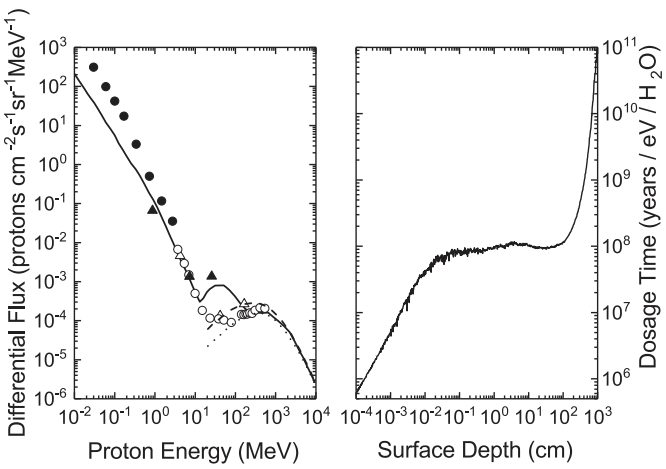

Fig. 9. Left: Proton differential flux model (solid curve) derived from spacecraft measurements (various symbols) at 30–50 AU and modulated spectra near solar minimum activity for galactic cosmic ray protons (dashed and dotted curves). Spacecraft measurements correspond to the following sources: Pioneer 10 Cosmic Ray Telescope (Δ), Voyager 2 Cosmic Ray Subsystem (○), Voyager 2 Low Energy Charged Particle Experiment measurements of protons (▲) and total ions (●). Right: Time to accumulate an absorbed energy dose of 1 eV per H_2O molecule at a specified surface depth, assuming a surface ice density of 1 g cm^{-3}. See Appendix A for more details.

presence of higher-energy galactic cosmic ray protons above 100 MeV. The thickness ~ 1 m of the constant dose region roughly corresponds to the nuclear interaction lengths of the high-energy protons and the electromagnetic interaction lengths of secondary protons, neutrons, electrons, positrons, muons and gamma rays. At larger depths, there is an exponential increase in dosage times as primary and secondary particle fluxes are attenuated in the upper layers. At some depth we have not yet determined, the natural radioactivity of mineral contaminants, e.g. ^{40}K, limits the maximum dosage time. It is important to point out that the radiation effects induced by cosmic rays, secondary particles produced by higher-energy cosmic rays, and our low energy electrons are expected to be similar after scaling to the absorbed dose. All these particles lose energy by producing thousands of ionizations and excitations as they pass through the solid, and many of these ionizations will ultimately produce secondary electrons, which deposit energy into and drive the observed changes in the target medium.

To properly evaluate whether we should expect crystalline-H_2O ice on the surface of these objects, we consider the depth probed by near-infrared spectroscopy, where crystalline H_2O-ice has been detected. A conservative estimate for this depth is ~100 μm (10^{-2} cm), as the expected depth of penetration by solar radiation at near-infrared wavelengths is on the order of tens of microns. At this depth, we estimate that it will take ~5×10^7 yrs. to reach the dose needed to amorphize half of the surface (~1 eV molecule^{-1}) and ~ 1.3×10^9 yrs. (~20–30 eV molecule^{-1}) for complete amorphization if we only consider the 3.1 μm absorption feature. However, the timescale for complete amorphization could be a factor of two to three longer if we consider the results from our 1.65 μm absorption band study (see Fig. 7 bottom). We point out that these time estimates are ~two orders of magnitude longer than was given previously (Jewitt and Luu, 2004), as only the time to alter the top 100 nm was considered. However, they are consistent with estimates made by Pinilla-Alonso et al. (2009), who estimated the surface of Haumea could be best fit with a ~ 1:1 mixture of amorphous and crystalline H_2O-ice.

It is possible that our time estimates could be shortened if other components of the radiation flux are included besides the dominant proton component, as has been suggested for other extraterrestrial environments (Bringa et al., 2007; Raut et al., 2008). Nonetheless, given that these estimates are probably no better than a factor of two, we conclude that the time needed to amorphize crystalline H_2O-ice with a surface temperature near 50 K is surprisingly close to the age of the solar system. Thus, detecting a crystalline or partially crystalline H_2O-ice surface in the outer solar system, may not be that surprising, especially considering impact events, such as those by micrometeorites, are likely to refresh the surface during the icy object's lifetime.

5. Conclusions

We have measured the amorphization of crystalline H_2O-ice for 1–10 keV electrons at 50 K and 1 keV electrons between 10 and 100 K, using infrared spectroscopy as an analytical tool. We find that at all the energies studied, electrons can amorphize crystalline H_2O-ice and the fluence needed for amorphization is ~10 times lower in samples irradiated with 1 keV electrons than with 10 keV electrons. However, after scaling experiments to the total energy absorbed in the sample, i.e. by plotting the amorphous fraction vs. absorbed dose, we find that the 1, 2 and 5 keV experiments produce curves that are within 10% of one another, while the 10 keV experiments are within 50% of the other experiments, supporting previous suggestions that the main variable driving amorphization at low temperatures is the total energy absorbed in the sample. In addition, comparing experiments with crystalline H_2O-ice samples about ~40 times different in thickness, we find that analysis of the amorphous fraction using either the 1.65 μm or 3.1 μm absorption band produces similar results. Finally, using 1 keV electrons we also find that we can completely amorphize crystalline H_2O-ice at temperatures as high as 70 K and the rate of amorphization increases significantly as the irradiation temperature is decreased. Above 70 K, we find that the total fraction of the sample that can be amorphized decreases rapidly.

Generally, our results suggest that any icy body existing at temperatures lower than 70 K will be amorphized, assuming the flux of energetic electrons at the surface is sufficient. Of course, given the similarity observed in our experiments compared with the previous ones involving other energetic particles, we suspect that any surface exposed to radiation will be amorphized at these low temperatures given enough time. However, for the specific question of the presence of crystalline-H_2O on Kuiper Belt Objects, we estimate that the time needed to completely amorphize the material to the depth probed by near-infrared spectroscopy is nearly the age of the solar system. Given the uncertainties involved in these types of extrapolations and the possibility of a resurfacing event occurring in these objects' lifetimes, the detection of crystalline or at least partially crystalline H_2O-ice on their surface should be expected.

Data availability

=Data from this publication can be found in Northern Arizona University's long-term repository (https://openknowledge.nau.edu/5515/).

Acknowledgements

This research was supported by NSF Grant # 1821919.

Appendix A

We have compiled the proton flux model in Fig. 9 (left) for 10^{-2} - 10^4 MeV protons in the Kuiper Belt Object (KBO) region at 30–50 AU from a variety of data sources. The spacecraft source data points are from the Virtual Energetic Particle Observatory (VEPO) at https://vepo.gsfc.nasa.gov/ and are averaged for the years when measurements are taken in the KBO region, 1983–1991 for Pioneer 10 and 1989–1996 for Voyager 2. We do not include also-available Pioneer 11 and Voyager 1 data taken away from the Ecliptic. The bulge in the spectrum at 10–100 MeV is from contributions near solar minimum activity of "anomalous component" protons accelerated in the outer heliosphere. The two

dashed curves from Vos and Potgieter (2015) are for galactic cosmic ray (GCR) spectra also near minimum activity levels. There is a divergence in Voyager 2 LECP data points from the model for protons below 1 MeV, since the data are from total ion (H + He + …) measurements and we have extrapolated the proton model spectrum from higher-energy measurements

Modeling the dosage time vs. surface depth (Fig. 9 right) requires propagation of differential flux spectra into surfaces with the GEometry ANd Tracking Detector Description and Simulation Tool (GEANT (Brun et al., 1994, Cooper and Sturner, 2018)) radiation transport code. The 10^{-2}–10^{4} MeV incident protons are assumed to be isotropically incident onto a flat ice surface of sufficient depth that most of the energy deposition from primary and secondary radiation is contained. We did not include heavier primaries, as the main flux component at the 90% level comes from the protons.

References

Ashley, J.C., 1982. Stopping power of liquid water for low-energy electrons. Radiat. Res. 89, 25–31.

Baragiola, R.A., 2003. Water ice on outer solar system surfaces: basic properties and radiation effects. Planet. Spac. Sci. 51, 953–961.

Baratta, G.A., et al., 2002. A comparison of ion irradiation and UV photolysis of CH_4 and CH_3OH. Astron. Astrophys. 384, 343–349.

Beaumont, R.H., et al., 1961. Transitions between different forms of ice. J. Chem. Phys. 34, 1456–1457.

Berger, M.J., et al.. Stopping-Power and Range Tables for Electrons, Protons, and Helium Ions. http://www.nist.gov/pml/data/star/index.cfm.

Boring, J.W., et al., 1983. Ion-induced chemistry in condensed gas solids. Nuc. Instr. Met. Res. 218, 707–711.

Bringa, E.M., et al., 2007. Energetic processing of interstellar silicate grains by cosmic rays. Astrophys. J. 662, 372–378.

Bronshtein, I.M., Fraiman, B.S., 1969. Vtorichnaya Elektronnaya Emissiya (Secondary Electron Emission) (Nauka-Moskva).

Brown, M.E., Calvin, W.M., 2000. Evidence for crystalline water and ammonia ices on Pluto's satellite Charon. Science 287, 107–109.

Brun, R., et al., 1994. GEANT: detector description and simulation tool. In: CERN Program Library Long Writeup W5013. CERN (Conseil Européen pour la Recherche Nucléaire), Geneva, Switzerland.

Cooper, J.F., Sturner, S.J., 2018. Energetic radiation from galactic cosmic ray interactions with Saturn's main rings. J. Geophys. Res. 123, 7473–7485.

Cooper, J.F., et al., 2001. Energetic ion and electron irradiation of the icy Galilean satellites. Icarus 149, 133–159.

Cooper, J.F., et al., 2003. Proton irradiation of Centaur, Kuiper Belt, and Oort Cloud objects at plasma to cosmic ray energy. Earth Moon Planet. 92, 261–277.

Cooper, J.F., et al., 2009. Old faithful model for radiolytic gas-driven cryovolcanism at Enceladus. Planet. Space Sci. 57, 1607–1620.

Cruikshank, D.P., 1980. Near-infrared studies of the satellites of Saturn and Uranus. Icarus 41, 246–258.

Dubochet, J., Lepault, J., 1984. Cryo-electron microscopy of vitrified water. J. Phys. 45, 85–94.

El Gomati, M.M., et al., 2008. Theory experiment comparison of the electron backscattering factor from solids at low electron energy (250-5,000 eV). Scanning 30, 2–15.

Famá, M., et al., 2010. Radiation-induced amorphization of crystalline ice. Icarus 207, 314–319.

Fink, U., et al., 1976. Infrared-spectra of satellites of Saturn - identification of water ice on Iapetus, Rhea, Dione, and Tethys. Astrophys. J. 207, L63–L67.

Francis, Z., et al., 2011. Stopping power and ranges of electrons, protons and alpha particles in liquid water using the Geant4-DNA package. Nucl. Instrum. Meth. Phys. Res. B 269, 2307–2311.

Gerakines, P.A., et al., 2004. Ultraviolet photolysis and proton irradiation of astrophysical ice analogs containing hydrogen cyanide. Icarus 170, 202–213.

Ghormley, J.A., 1968. Enthalpy changes and heat-capacity changes in transformations from high-surface-area amorphous ice to stable hexagonal ice. J. Chem. Phys. 48, 503–508.

Golecki, I., Jaccard, C., 1978. Radiation damage in ice at low temperatures studied by proton channeling. J. Glaciol. 21, 247–258.

Grundy, W.M., et al., 1999. Near-infrared spectra of icy outer solar system surfaces: remote determination of H_2O ice temperatures. Icarus 142, 536–549.

Heavens, O.S., 1965. Optical Properties of Thin Solid Films. Dover Publications, Inc., New York.

Heide, H.G., 1984. Observations on ice layers. Ultramicroscopy 14, 271–278.

Hudson, R.L., Moore, M.H., 2001. Radiation chemical alterations in solar system ices: an overview. J. Geophys. Res. 106, 33275–33284.

Hudson, R.L., et al., 2008. Laboratory studies of the chemistry of TNO surface materials. In: Barucci, A., Boehnhardt, H., Cruikshank, D.P., Morbidelli, A. (Eds.), The Solar System Beyond Neptune. Univ. of Arizona Press, Tucson, Arizona, pp. 507–523.

Jenniskens, P., Blake, D.F., 1996. Crystallization of amorphous water ice in the solar system. Astrophys. J. 473, 1104–1113.

Jewitt, D.C., Luu, J., 2004. Crystalline water ice on the Kuiper Belt Object (50000) Quaoar. Nature 432, 731–733.

Kouchi, A., Kuroda, T., 1990. Amorphization of cubic ice by ultraviolet-irradiation. Nature 344, 134–135.

Lepault, J., et al., 1983. Electron-beam induced vitrified ice. J. Micro. 132, Rp3–Rp4.

Leto, G., et al., 2005. The reflectance spectrum of water ice: is the 1.65 μm peak a good temperature probe? Mem. Soc. Astron. Ital. Suppl. 6, 57–62.

Leto, G., Baratta, G.A., 2003. Lyman alpha photon induced amorphization of I_c water ice at 16 kelvin. Effects and quantitative comparison with ion irradiation. Astron. Astrophys. 397, 7–13.

Loeffler, M.J., Baragiola, R.A., 2009. Physical and chemical effects on crystalline H_2O_2 induced by 20 keV protons. J. Chem. Phys. 130, 114504.

Loeffler, M.J., et al., 2005. CO_2 synthesis in solid CO by Lyman-alpha photons and 200 keV protons. Astron. Astrophys. 435, 587–594.

Loeffler, M.J., et al., 2015. Giant-planet chemistry: ammonium hydrosulfide (NH_4SH), its IR spectra and thermal and radiolytic stabilities. Icarus 258, 181–191.

Mastrapa, R.M.E., Brown, R.H., 2006. Ion irradiation of crystalline H_2O-ice: effect on the 1.65 micron band. Icarus 183, 207–214.

Meier, R.M., Loeffler, M.J., 2020. Sputtering of water ice by keV electrons at 60 K. Surf. Sci. 691, 121509.

Merlin, F., et al., 2007. Properties of the icy surface of the TNO 136108 (2003 EL61). Astron. Astrophys. 466, 1185–1188.

Moore, M., Hudson, R., 1992. Far-infrared spectral studies of phase changes in water ice induced by proton irradiation. Astrophys. J. 401, 353–360.

Olander, D.S., Rice, S.A., 1972. Preparation of amorphous solid water. Proc. Natl. Acad. Sci. 69, 98–100.

Pilcher, C.B., et al., 1972. Galilean satellites - identification of water frost. Science 178, 1087–1089.

Pinilla-Alonso, N., et al., 2009. The surface of (136108) Haumea (2003 EL61), the largest carbon-depleted object in the trans-Neptunian belt. Astron. Astrophys. 496, 547–556.

Pryde, J.A., Jones, G.O., 1952. Properties of vitreous water. Nature 170, 685–688.

Raut, U., et al., 2008. Cosmic ray compaction of porous interstellar ices. Astrophys. J. 687, 1070–1074.

Reimann, C.T., et al., 1984. Ion-induced molecular ejection from D_2O ice. Surf. Sci. 147, 227–240.

Sceats, M.G., Rice, S.A., 1982. Water and aqueous solutions at subzero temperatures: amorphous solid water and its relationship to liquid water: a random network model for water. In: Franks, F. (Ed.), Water, A Comprehensive Treatise. Plenum, New York, pp. 83–214.

Strazzulla, G., et al., 1992. Ion-beam-induced amorphization of crystalline water ice. Europhys. Lett. 18, 517–522.

Strazzulla, G., et al., 2003. Ion irradiation of TNOs: from the fluxes measured in space to the laboratory experiments. Comp. Rend. Phys. 4, 791–801.

Szenes, G., 1995. General features of latent track formation in magnetic insulators irradiated with swift heavy-ions. Phys. Rev. B 51, 8026–8029.

Teolis, B.D., et al., 2005. Mechanisms of O_2 sputtering from water ice by keV ions. Phys. Rev. B 72, 245422.

Teolis, B.D., et al., 2009. Formation, trapping, and ejection of radiolytic O_2 from ion-irradiated water ice studied by sputter depth profiling. J. Chem. Phys. 130, 134704.

Trujillo, C.A., et al., 2007. The surface of 2003 EL61 in the near-infrared. Astrophys. J. 655, 1172–1178.

Vos, E.E., Potgieter, M.S., 2015. New modeling of galactic proton modulation during the minimum of solar cycle 23/24. Astrophys. J. 815, 119.

Walker, C.G.H., et al., 2008. The secondary electron emission yield for 24 solid elements excited by primary electrons in the range 250-5000 eV: a theory/experiment comparison. Scanning 30, 365–380.

Zheng, W.J., et al., 2009. On the state of water ice on Saturn's moon Titan and implications to icy bodies in the outer solar system. J. Phys. Chem. A 113, 11174–11181.

Ziegler, J.F., 2010. Stopping and Range of Ions in Matter SRIM2010. available at. www.srim.org.